

## Articles

### Benzimidazole Derivatives. 3. 3D-QSAR/CoMFA Model and Computational Simulation for the Recognition of 5-HT<sub>4</sub> Receptor Antagonists

María L. López-Rodríguez,<sup>\*,†</sup> Marta Murcia,<sup>†</sup> Bellinda Benhamú,<sup>†</sup> Alma Viso,<sup>†</sup> Mercedes Campillo,<sup>‡</sup> and Leonardo Pardo<sup>\*,‡</sup>

*Departamento de Química Orgánica I, Facultad de Ciencias Químicas, Universidad Complutense, 28040 Madrid, Spain, and Laboratori de Medicina Computational, Unitat de Bioestadística, Facultat de Medicina, Universitat Autònoma de Barcelona, 08193 Bellaterra, Spain*

Received January 3, 2002

A three-dimensional quantitative structure–affinity relationship study (3D-QSAR), using the comparative molecular field analysis (CoMFA) method, and subsequent computational simulation of ligand recognition have been successfully applied to explain the binding affinities for the 5-HT<sub>4</sub> receptor (5-HT<sub>4</sub>R) of a series of benzimidazole-4-carboxamides and carboxylates derivatives **1–24**. The  $K_i$  values of these compounds are in the range from 0.11 to 10 000 nM. The derived 3D-QSAR model shows high predictive ability ( $q^2 = 0.789$  and  $r^2 = 0.997$ ). Steric (contribution of 43.5%) and electrostatic (50.3%) fields and solvation energy (6.1%) of this novel class of 5-HT<sub>4</sub>R antagonists are relevant descriptors for structure–activity relationships. Computational simulation of the complexes between the benzimidazole-4-carboxamide UCM-21195 (**5**) and the carboxylate UCM-26995 (**21**) and a 3D model of the transmembrane domain of the 5-HT<sub>4</sub>R, constructed using the reported crystal structure of rhodopsin, have allowed us to define the molecular details of the ligand–receptor interaction that includes (i) the ionic interaction between the NH group of the protonated piperidine of the ligand and the carboxylate group of Asp<sup>3.32</sup>, (ii) the hydrogen bond between the carbonyl oxygen of the ligand and the hydroxyl group of Ser<sup>5.43</sup>, (iii) the hydrogen bond between the NH group of Asn<sup>6.55</sup> and the aromatic ring of carboxamides or the ether oxygen of carboxylates, (iv) the interaction of the electron-rich clouds of the aromatic ring of Phe<sup>6.51</sup> and the electron-poor hydrogens of the carbon atoms adjacent to the protonated piperidine nitrogen of the ligand, and (v) the  $\pi$ – $\sigma$  stacking interaction between the benzimidazole system of the ligand and the benzene ring of Tyr<sup>5.38</sup>. Moreover, the noticeable increase in potency at the 5-HT<sub>4</sub>R sites, by the introduction of a chloro or bromo atom at the 6-position of the aromatic ring, is attributed to the additional electrostatic and van der Waals interaction of the halogen atom in a small cavity located between transmembrane domains 5 and 6.

#### Introduction

Since the discovery of the neurotransmitter serotonin (5-hydroxytryptamine, 5-HT) in 1948, the knowledge about its role in (patho)physiological processes, both peripherally and centrally, is steadily growing.<sup>1</sup> The actions of 5-HT are mediated by a number of specific receptors which have been classified into 7 classes (5-HT<sub>1–7</sub>) including 15 different subtypes.<sup>2–5</sup> The 5-HT<sub>4</sub> receptor (5-HT<sub>4</sub>R) is a member of the G-protein-coupled receptor (GPCR) superfamily, and it is positively linked to adenylyl cyclase in the central nervous system (CNS).<sup>6</sup> The 5-HT<sub>4</sub>Rs have been found in several animal and human peripheral tissues, such as the gastrointestinal tract,<sup>7–9</sup> the heart,<sup>10</sup> and the bladder<sup>11</sup> where they mediate a variety of pharmacological responses. Thus,

in addition to the clinical use of 5-HT<sub>4</sub>R agonists (cisapride, renzapride) as prokinetic agents in the treatment of gastrointestinal motility disorders,<sup>12,13</sup> a number of potential therapeutic indications for antagonists of this receptor are currently under investigation, including irritable bowel syndrome,<sup>14–16</sup> arrhythmias,<sup>17</sup> and micturition disturbances.<sup>18,19</sup> Moreover, the 5-HT<sub>4</sub>R facilitates the release of acetylcholine in the CNS, which suggests that 5-HT<sub>4</sub>R agonists may have a role in improving cognitive function.<sup>20</sup> In many cases, the clinical use of currently available drugs acting at the 5-HT<sub>4</sub>R has been hampered by their lack of selectivity, and significant efforts have been made toward the development of potent and selective 5-HT<sub>4</sub>R antagonists,<sup>21</sup> such as SDZ205–557, GR113808, SB204070, and RS39604 (see Figure 1).

In the course of a program aimed at the discovery of new 5-HT<sub>4</sub>R agents, we postulated a pharmacophore model for the recognition of 5-HT<sub>4</sub>R antagonists.<sup>22</sup> This model consists of an aromatic moiety, a coplanar carbonyl group, a protonated nitrogen atom, and a volu-

\* To whom correspondence should be addressed. For M. L. López-Rodríguez: (phone) 34-91-3944239; (fax) 34-91-3944103; (e-mail) mluzlr@quim.ucm.es. For L. Pardo: (phone) 3493-5812797; (fax) 3493-5812344; (e-mail) Leonardo.Pardo@uab.es.

<sup>†</sup> Universidad Complutense.

<sup>‡</sup> Universitat Autònoma de Barcelona.

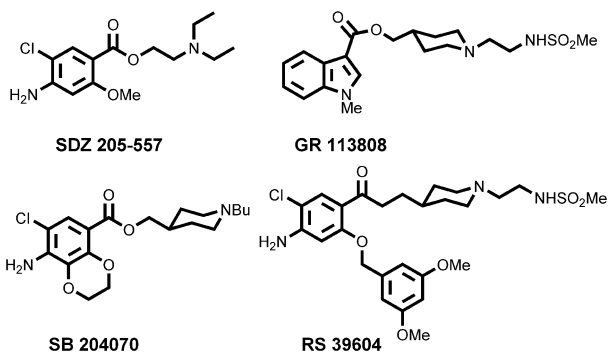
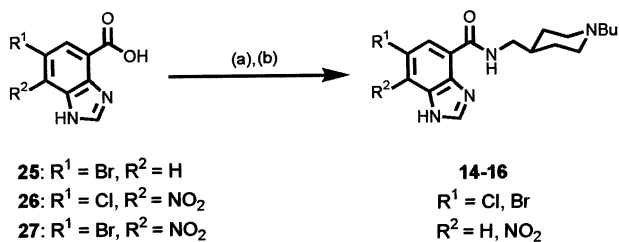


**Figure 1.** Chemical formulas of 5-HT<sub>4</sub>R antagonists.

**Scheme 1<sup>a</sup>**



<sup>a</sup> Reagents: (a) CDI, DMF, 40 °C; (b) (1-butyl-4-piperidyl)methylamine, DBU, DMF, 50 °C.

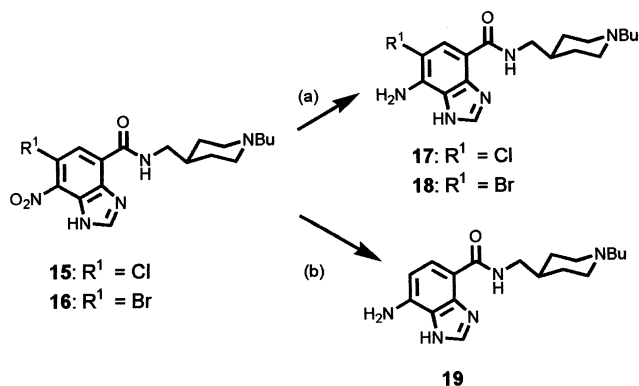
minous substituent in the basic amino framework of the molecule. This pharmacophore model led us to design a series of new benzimidazole-4-carboxylic acid derivatives, which were characterized as novel potent and selective 5-HT<sub>4</sub>R antagonists.<sup>23,24</sup> Furthermore, the amino acid residues of the human 5-HT<sub>4</sub>R involved in ligand binding have been identified by site-directed mutagenesis.<sup>25</sup> The structural interpretation of these experiments, in the context of molecular models of the transmembrane domain of the receptor constructed from the crystal structure of rhodopsin (RHO), has recently permitted us to define the amino acid side chains of the receptor that interact with the proposed pharmacophore elements;<sup>26</sup> the protonated nitrogen group forms an ionic interaction with Asp<sup>3.32</sup> (nomenclature of Ballesteros and Weinstein<sup>27</sup>), the carbonylic oxygen forms a hydrogen bond with Ser<sup>5.43</sup>, the aromatic moiety forms  $\pi$ - $\sigma$  aromatic-aromatic interactions with Phe<sup>6.52</sup> or Tyr<sup>5.38</sup>, and the voluminous substituent extends toward helix 7 of the receptor.

In this work we have synthesized new related analogues<sup>28</sup> and carried out both 3D-QSAR studies<sup>29</sup> using the comparative molecular field analysis (CoMFA)<sup>30,31</sup> methodology and computational models of the complexes between these ligands and the transmembrane domain of the receptor to rationalize the structure-affinity relationships of benzimidazole derivatives **1–24** acting at the 5-HT<sub>4</sub>R.

**Materials and Methods**

Compounds **1–13** and **20–24** were obtained previously in our group.<sup>24,32</sup> New amides **14–16** were synthesized from benzimidazole-4-carboxylic acids **25–27**<sup>33</sup> as detailed in Scheme 1. 7-Aminocarboxamides **17–19** were prepared from their corresponding 7-nitro derivatives. Thus, the treatment of **15** or **16** with hydrazine and Raney nickel yielded **17** and **18**, respectively, while reduction of **16** with hydrazine and palladium on carbon

**Scheme 2<sup>a</sup>**

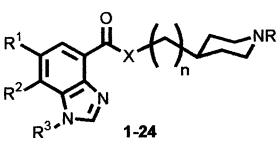


<sup>a</sup> Reagents: (a) NH<sub>2</sub>NH<sub>2</sub>, Raney Ni, EtOH, room temp; (b) (16) NH<sub>2</sub>NH<sub>2</sub>, Pd(C), EtOH,  $\Delta$ .

led to the heterolytic reduction of the C–Br bond to give **19** (Scheme 2). All new compounds (Table 1) were characterized by IR and <sup>1</sup>H and <sup>13</sup>C NMR spectroscopy and gave satisfactory combustion results (C, H, N).

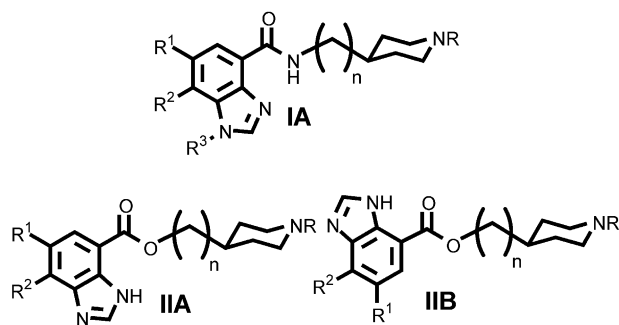
**5-HT<sub>4</sub> Affinities.** Target compounds were assessed for in vitro affinity at 5-HT<sub>4</sub>R<sub>s</sub> by radioligand binding assays, using [<sup>3</sup>H]GR113808 in rat striatum membranes<sup>34</sup> (Table 1). In the experimental binding assays, the compounds were first tested at fixed dose of 10<sup>–6</sup> M, and for only those that in the screening process presented high activity (displacement of the radioligand  $\geq 55\%$ ), the dose–response curves were determined. The inhibition constant *K*<sub>i</sub> was defined from the IC<sub>50</sub> using the Cheng–Prusoff equation.<sup>35</sup>

**3D-QSAR/CoMFA Method.** The identification of the bioactive conformation of the compounds under investigation is a crucial step in CoMFA. The benzimidazole ring can exist in two different tautomeric forms depending on whether the N<sub>1</sub> (tautomer **I**) or N<sub>3</sub> (tautomer **II**) nitrogen of the ring holds the hydrogen (see Figure 2). Moreover, the carbonyl group at the 4-position of the benzimidazole ring might adopt two rotamer conformations: cis (rotamer **A**) or trans (rotamer **B**) relative to the C<sub>4</sub>–C<sub>5</sub> bond of the benzimidazole ring (see Figure 2). Previous studies using NMR and IR techniques and theoretical calculations have reported structure **IA** of carboxamides and structure **IIB** of carboxylates as the most stable in solution.<sup>32</sup> Structure **IA** of carboxamides is stabilized by a hydrogen bond between the N<sub>3</sub> atom of the benzimidazole ring and the NH of the carboxamide group, whereas structure **IIB** of carboxylates forms a hydrogen bond between the N<sub>3</sub>–H moiety of the benzimidazole ring and the carbonyl of the carboxylate group. Accordingly, structure **IIB** of carboxylates contains a buried carbonyl group, in contrast to structure **IA** of carboxamides, which possesses a free carbonyl group that might act as a hydrogen bond acceptor in the interaction with the receptor. Structure–activity relationships and mutagenesis experiments suggest that the carbonyl group is a key pharmacophoric element for the recognition of 5-HT<sub>4</sub> antagonists.<sup>22,25,26,32</sup> Thus, we have considered rotamer **A** of the carbonyl group as the bioactive conformation of benzimidazole derivatives **1–24**. In consequence, carboxylates must undergo a conformational change to rotamer **A** to interact with the receptor. The energy required for this conformational change was estimated to be 1.1 kcal mol<sup>–1</sup> in solution for UCM-26995 (**21**).<sup>32</sup>

**Table 1.** Experimental and CoMFA-Predicted 5-HT<sub>4</sub>R Binding Affinities of Benzimidazole Derivatives 1–24


compd	R <sup>1</sup>	R <sup>2</sup>	R <sup>3</sup>	X	n	R	K <sub>i</sub> ± SEM <sup>a</sup> (nM)	pK <sub>i</sub> <sup>e</sup> (M)	pK <sub>i</sub> <sup>pred e</sup> (M)
<b>1</b>	H	H	H	NH	0	Me	719 ± 58	6.14	6.38 <sup>#</sup>
<b>2</b>	H	H	H	NH	0	Et	>1000	6.00 <sup>§</sup>	5.91
<b>3</b>	H	H	H	NH	0	Pr	>1000	6.00 <sup>§</sup>	6.02
<b>4</b>	H	H	H	NH	0	Bu	290 ± 54	6.54 <sup>§</sup>	6.61
<b>5<sup>b</sup></b>	H	H	H	NH	1	Bu	13.7 ± 0.9	7.86 <sup>§</sup>	7.97
<b>6</b>	H	H	H	NH	1	MSAE <sup>d</sup>	11.4 ± 3.0	7.94 <sup>§</sup>	7.94
<b>7</b>	Cl	H	H	NH	0	Me	54.0 ± 2.8	7.27 <sup>§</sup>	7.36
<b>8</b>	Cl	H	H	NH	1	Bu	0.32 ± 0.07	9.49 <sup>§</sup>	9.32
<b>9</b>	Cl	H	H	NH	1	MSAE <sup>d</sup>	0.11 ± 0.03	9.96 <sup>§</sup>	9.99
<b>10</b>	Cl	H	H	NH	1	<sup>t</sup> Bu	0.29 ± 0.04	9.54 <sup>§</sup>	9.46
<b>11</b>	Cl	H	H	NH	1	pent	0.54 ± 0.10	9.27 <sup>§</sup>	9.26
<b>12</b>	Cl	H	CH <sub>2</sub> Ph	NH	1	<sup>t</sup> Bu	69.2 ± 9.3	7.16 <sup>§</sup>	7.19
<b>13</b>	Cl	H	Me	NH	1	<sup>t</sup> Bu	2.2 ± 0.2	8.66 <sup>§</sup>	8.66
<b>14</b>	Br	H	H	NH	1	Bu	0.64 ± 0.04	9.19 <sup>§</sup>	9.17
<b>15</b>	Cl	NO <sub>2</sub>	H	NH	1	Bu	44.6 ± 2.0	7.35	7.59 <sup>#</sup>
<b>16</b>	Br	NO <sub>2</sub>	H	NH	1	Bu	48.2 ± 6.5	7.32 <sup>§</sup>	7.32
<b>17</b>	Cl	NH <sub>2</sub>	H	NH	1	Bu	22.4 ± 0.6	7.65 <sup>§</sup>	7.75
<b>18</b>	Br	NH <sub>2</sub>	H	NH	1	Bu	27.8 ± 3.3	7.56 <sup>§</sup>	7.63
<b>19</b>	H	NH <sub>2</sub>	H	NH	1	Bu	115 ± 15	6.94 <sup>§</sup>	6.85
<b>20</b>	H	H	H	O	0	Me	>10000	5.00 <sup>§</sup>	4.91
<b>21<sup>c</sup></b>	H	H	H	O	1	Bu	24.6 ± 0.5	7.61 <sup>§</sup>	7.59
<b>22</b>	H	H	H	O	1	MSAE <sup>d</sup>	26.1 ± 0.0.3	7.58 <sup>§</sup>	7.59
<b>23</b>	Cl	H	H	O	1	Bu	2.9 ± 0.4	8.54	8.39 <sup>#</sup>
<b>24</b>	Cl	H	H	O	1	MSAE <sup>d</sup>	2.3 ± 1.1	8.64 <sup>§</sup>	8.67

<sup>a</sup> K<sub>i</sub> values are mean ± SEM of two to four assays performed in triplicate. Inhibition curves were analyzed by a computer-assisted curve-fitting program (Prism GraphPad), and K<sub>i</sub> values were determined from the Cheng–Prusoff equation. <sup>b</sup> 5: UCM-21195. <sup>c</sup> 21: UCM-26995. <sup>d</sup> MSAE: [(methylsulfonyl)amino]ethyl. <sup>e</sup> (S) Compounds of the training set used to develop the CoMFA model. (#) Compounds used to test the CoMFA model.

**1-24**

R<sup>1</sup> = H, Cl, Br; R<sup>2</sup> = H, NO<sub>2</sub>, NH<sub>2</sub>;  
 R<sup>3</sup> = H, Me, CH<sub>2</sub>Ph;  
 n = 0, 1; R = Me, Et, Pr, Bu, Bu<sup>t</sup>,  
 Pent, (CH<sub>2</sub>)<sub>2</sub>NHSO<sub>2</sub>Me

**Figure 2.** Benzimidazole derivatives acting at the 5-HT<sub>4</sub>R.

The equilibrium structures of the piperidine-protonated form of derivatives 1–24 were obtained by full geometry optimization with the AM-1 Hamiltonian model. The initial conformation of the side chain of compounds 5, 6, 8–19, 21–24, all of which possess a methylene unit between the piperidine ring and the carboxamide or carboxylate moieties, was selected from the conformation of UCM-21195 (5) or UCM-26995 (21) in their complex with the transmembrane domain of the 5-HT<sub>4</sub>R (see below and Results and Discussion). The initial conformation of the less flexible compounds 1–4, 7, and 20 without this methylene unit was chosen in such a way that their benzimidazole and piperidine rings had similar arrangements in space than the

methylene-containing compounds. The entire set of compounds was oriented in space by superimposing the heavy atoms of the common and rigid benzimidazole ring and the piperidine moiety, using UCM-21195 (5) as the reference compound. The atom-centered atomic charges used in CoMFA to evaluate the electrostatic field were computed from the molecular electrostatic potential<sup>36</sup> using the 6-31G\* basis set, a common procedure for simulation of proteins, nucleic acids, and organic molecules.<sup>37</sup> Solvation free energies ( $\Delta G_{\text{solv}}$ ) of the isolated ligands were calculated with a polarized continuum model using the 6-31G\* basis set. K<sub>i</sub> is a function of both the stabilization of the complex formed between the ligand molecule and the receptor and the solvation energy of the ligand. Thus, the QSAR table for the CoMFA study consisted of the pK<sub>i</sub> values (dependent variable) and the steric and electrostatic fields (independent variables), to mimic the stabilization energy of the ligand–receptor complex, and  $\Delta G_{\text{solv}}$  (independent variable). The steric and electrostatic potential fields were calculated at each lattice intersection of a regularly spaced grid of 2 Å. An sp<sup>3</sup> carbon atom with a van der Waals radius of 1.52 Å carrying a charge of +1.0 served as a probe atom to calculate steric and electrostatic fields. The steric and electrostatic contributions were truncated to ±30 kcal mol<sup>-1</sup>, and the electrostatic contributions were ignored at lattice intersections with maximal steric interactions. Partial least-squares (PLS) analysis<sup>38–41</sup> was used to derive linear equations from the resulting matrices. Leave one out (LOO) cross-validation was employed to select the number of principal components and to calculate the

cross-validated statistics. The final CoMFA model was generated using non-cross-validation and the number of components suggested by the LOO validation run. The 3D-QSAR/CoMFA study was carried out with the QSAR module of the SYBYL 6.5 program,<sup>42</sup> using default parameters. All the quantum mechanical calculations were performed with the Gaussian 98 system of programs.<sup>43</sup>

**Models of 5-HT<sub>4</sub>R–Ligand Interaction.** The 3D model of the transmembrane domain of the 5-HT<sub>4</sub>R was constructed by computer-aided model building techniques from the transmembrane domain (HELIX annotation in the 1F88 PDB file) of the recently reported<sup>44</sup> crystal structure of RHO. Conserved residues Asn<sup>55</sup> (residue number in the PDB file of RHO) and Asn<sup>37</sup> (residue number in the human 5-HT<sub>4</sub>R sequence) (Asn<sup>1.50</sup> in the generalized numbering scheme,<sup>27</sup> Asp<sup>83</sup> and Asp<sup>66</sup> (Asp<sup>2.50</sup>), Arg<sup>135</sup> and Arg<sup>118</sup> (Arg<sup>3.50</sup>), Trp<sup>161</sup> and Trp<sup>146</sup> (Trp<sup>4.50</sup>), Pro<sup>215</sup> and Pro<sup>204</sup> (Pro<sup>5.50</sup>), Pro<sup>267</sup> and Pro<sup>274</sup> (Pro<sup>6.50</sup>), and Pro<sup>303</sup> and Pro<sup>309</sup> (Pro<sup>7.50</sup>)) were employed in the alignment of RHO and human 5-HT<sub>4</sub>R transmembrane sequences. All ionizable residues in the helices were considered uncharged with the exception of Asp<sup>2.50</sup>, Asp<sup>3.32</sup>, Asp<sup>3.49</sup>, Arg<sup>3.50</sup>, and Glu<sup>6.30</sup>. SCWRL-2.1 was employed to add the side chains of the non-conserved residues based on a backbone-dependent rotamer library.<sup>45</sup> A bending angle of 4°<sup>46</sup> has been incorporated in TMH 3 at position 3.37, facilitating the experimentally derived interactions between the ligand and Asp<sup>3.32</sup> and Ser<sup>5.43</sup>, because Thr<sup>3.37</sup> adopts the gauche-conformation during the molecular modeling procedure. In this conformation, Ser and Thr residues induce a small bending angle in transmembrane helices.<sup>46</sup> Gauche is the only allowed conformation of Thr<sup>3.37</sup> because of the steric clash between the methyl group and either the carbonyl oxygen of residue *i* – 3, in *trans* or the atoms of Pro<sup>4.53</sup> in *gauche*+. We have recently provided experimental evidence for this structural difference of TMH 3 in RHO and the serotonin family of GPCRs by designing and testing ligands that contain comparable functional groups but at different interatomic distances.<sup>47</sup>

The mode of recognition of the ligands was first determined by ab initio geometry optimization with the 3-21G basis set. The model system consisted of Asp<sup>3.32</sup>, Ser<sup>5.43</sup>, and Asn<sup>6.55</sup> (only the C<sub>α</sub> atom of the backbone is included) of 5-HT<sub>4</sub>R and the ligands UCM-21195 (**5**) and UCM-26995 (**21**) (the butyl group attached to the piperidine nitrogen was replaced by a methyl group). All free valences were capped with hydrogen atoms. The C<sub>α</sub> atoms of the residues were kept fixed at the positions previously obtained (see above). These optimized, reduced models of the ligand–receptor complexes were used to position UCM-21195 (**5**) and UCM-26995 (**21**) inside the previously obtained transmembrane domain of the 5-HT<sub>4</sub>R. Subsequently, the complete system was energy-minimized.

Quantum mechanical calculations were performed with the Gaussian 98 system of programs.<sup>43</sup> Energy minimization was run with the Sander module of AMBER5,<sup>48</sup> an all-atom force field,<sup>37</sup> and a 13 Å cutoff for nonbonded interactions. Parameters for UCM-21195 (**5**) and UCM-26995 (**21**) were adapted from Cornell et al.'s force field<sup>37</sup> using RESP point charges.<sup>49</sup>

**Table 2.** Statistical Results of the Generated 5-HT<sub>4</sub> CoMFA Model<sup>a</sup>

$q^2$	0.789
SEP	0.772
<i>n</i>	8
<i>N</i>	21
$r^2$	0.997
SEE	0.093
<i>F</i>	485.248
<i>p</i>	0.000
contributions	
steric, %	43.5
electrostatic, %	50.3
solvation ( $\Delta G_{\text{solv}}$ ), %	6.1

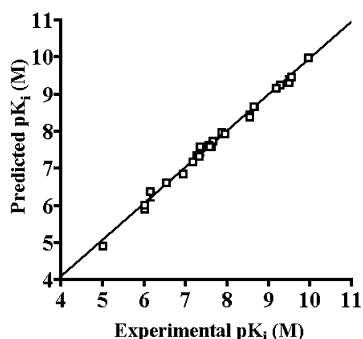
<sup>a</sup> Statistical properties of PLS model using steric and electrostatic CoMFA fields and  $\Delta G_{\text{solv}}$  as independent variables. The LOO cross-validated  $r^2$  value is denoted  $q^2$ . SEP is the standard error of prediction. *N* is the number of principal components used in the PLS analysis. *n* is the number of compounds.  $r^2$  is the non-cross-validated value. SEE is the standard error of estimation. *F* is the *F* statistic for the analysis. *p* is the probability of  $r^2 = 0$ , and contributions give the relative percentage of contribution of the field or  $\Delta G_{\text{solv}}$ .

## Results and Discussion

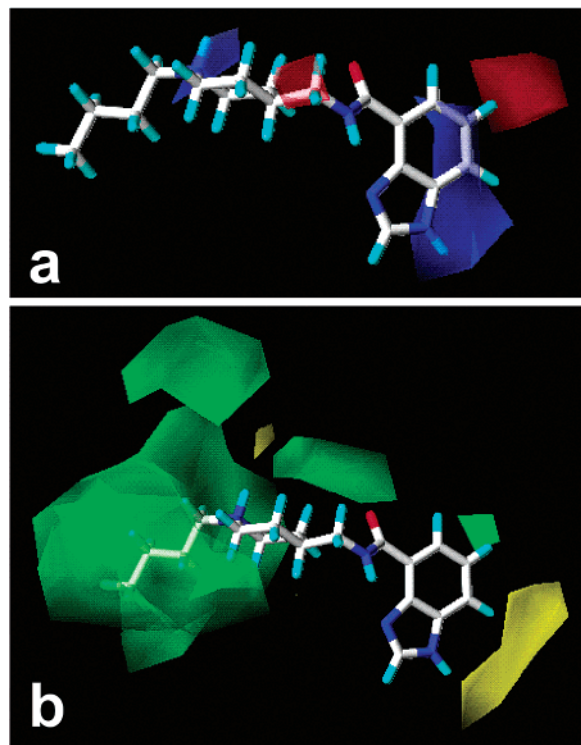
**3D-QSAR/CoMFA Model.** 3D-QSAR/CoMFA analysis was performed on the benzimidazole-4-carboxamides and carboxylates **1–24** (see Table 1), characterized as 5-HT<sub>4</sub>R antagonists. The tautomeric form of the benzimidazole ring and the conformation of the carbonyl group at the 4-position of the benzimidazole ring were selected from our previous structural analysis<sup>32</sup> of the annular tautomerism in these benzimidazole derivatives in solution, by using NMR and IR techniques and theoretical calculations (see Materials and Methods). The CoMFA model was developed using a training set of 21 compounds marked with § in Table 1. Randomly chosen compounds **1**, **15**, and **23** were not included in this training set in order to test the derived CoMFA model predictiveness. Thus, the binding affinities expressed as p*K*<sub>i</sub> (M) toward 5-HT<sub>4</sub>R of the training set were related to the independent variables (steric and electrostatic fields and solvation energies) by the PLS methodology.<sup>38–41</sup>

Table 2 shows the statistical properties of the model. The CoMFA-derived QSAR model shows a high LOO cross-validated  $r^2$  ( $q^2 = 0.789$ ) and therefore is a useful tool for predicting the 5-HT<sub>4</sub>R affinities. In addition, the model yielded a conventional  $r^2$  of 0.997 (eight principal components). Steric and electrostatic fields and  $\Delta G_{\text{solv}}$  contribute 43.5%, 50.3%, and 6.1%, respectively, to the QSAR equation. As a further test of robustness, the CoMFA model was applied to the excluded ligands **1**, **15**, and **23**. Clearly the theoretically predicted p*K*<sub>i</sub> values (see # symbol in Table 1) are in agreement with the experimentally determined values. The quality of the CoMFA model is also illustrated in Figure 3, which displays a plot between predicted p*K*<sub>i</sub> and observed p*K*<sub>i</sub> (correlation coefficient  $r^2 = 0.9938$ ) for the whole set compounds **1–24**. The theoretically predicted p*K*<sub>i</sub> values are also listed in Table 1.

Figure 4 illustrates the CoMFA electrostatic and steric maps using compound UCM-21195 (**5**) as the reference structure. Figure 4a shows areas where a high electron density provided by the ligand increases (red) or decreases (blue) the binding affinity. In Figure 4b, green areas depict zones of the space where occupancy



**Figure 3.** Plot of the predicted  $pK_i$  versus the experimental  $pK_i$  values for the 5-HT<sub>4</sub> CoMFA model ( $n = 24$ ,  $r^2 = 0.9938$ ). Residuals are shown as error bars.



**Figure 4.** Electrostatic and steric CoMFA maps showing contributions to 5-HT<sub>4</sub> affinity (plotted as percentage contribution to the QSAR equation). To visualize the CoMFA steric and electrostatic fields, contour maps of the product of the standard deviation associated with the CoMFA column and coefficient ( $SD \times \text{coeff}$ ) at each lattice point were generated. The color code is as follows. (a) For the electrostatic map, red denotes regions where positive charge is detrimental to affinity and blue denotes regions where positive charge enhances the affinity. (b) For the steric map, yellow denotes regions where steric bulk is detrimental to affinity and green denotes regions where steric bulk enhances the affinity. Compound UCM-21195 (**5**) is shown for reference.

by the ligands increases affinity, whereas yellow areas depict zones where occupancy decreases affinity.

The CoMFA analysis allowed us to rationalize the observed data of 5-HT<sub>4</sub>R binding affinities. The electrostatic and steric maps show a high electron density in the red region and a small favorable (green) area at the 6-position of the benzimidazole ring. These regions are indicative of the favorable effect, both electrostatic and steric, of the introduction of a chloro or bromo atom at the 6-position of the aromatic ring, which induces a notable increase in potency at 5-HT<sub>4</sub>R [ $K_i$ (**5**) = 13.7 nM

vs  $K_i$ (**8**) = 0.32 nM vs  $K_i$ (**14**) = 0.64 nM;  $K_i$ (**6**) = 11.4 nM vs  $K_i$ (**9**) = 0.11 nM;  $K_i$ (**21**) = 24.6 nM vs  $K_i$ (**23**) = 2.9 nM;  $K_i$ (**22**) = 26.1 nM vs  $K_i$ (**24**) = 2.3 nM]. It is important to note that the addition of the chloro atom does not have the same effect in carboxamides as in carboxylates. The effect of this addition in the binding affinity (monitored by the ratio of  $K_i$  values) is larger for carboxamides (42.8 for **5** vs **8**; 103.6 for **6** vs **9**) than for carboxylates (8.5 for **21** vs **23**; 11.3 for **22** vs **24**). These findings suggest that there might be a small cavity at the binding site of the 5-HT<sub>4</sub>R. The orientation of the chloro atom inside this cavity seems slightly different for both types of compound and more favorable for carboxamide derivatives. This different position of the chloro atom seems to be due to the different mode of binding of the carboxamide and carboxylate moieties of the ligands to the side chain of Asn<sup>6.55</sup> (see Molecular Model of the 5-HT<sub>4</sub>R–Ligand Interaction).

The substituent at the 7-position of the benzimidazole ring is also critical for ligand binding. The amino or nitro substitution at the 7-position induces a detrimental effect on affinity [e.g.,  $K_i$ (**5**) = 13.7 nM vs  $K_i$ (**19**) = 115 nM;  $K_i$ (**8**) = 0.32 nM vs  $K_i$ (**15**) = 44.6 nM vs  $K_i$ (**17**) = 22.4 nM;  $K_i$ (**14**) = 0.64 nM vs  $K_i$ (**16**) = 48.2 nM vs  $K_i$ (**18**) = 27.8 nM]. Accordingly, the electrostatic map (see Figure 4a) shows a blue area in the vicinity of this position, reflecting that the high electron density provided by the amino or nitro substituents decreases binding affinity, and the steric map (see Figure 4b) displays a yellow (unfavorable) area, which would be occupied by these substituents.

Similarly, methylation of the 1-N of the benzimidazole carboxamide **10** produces a reduction on the 5-HT<sub>4</sub> affinity [ $K_i$ (**10**) = 0.29 nM vs  $K_i$ (**13**) = 2.2 nM]. The energy cost of desolvating the N<sub>1</sub>–H ligand ( $\Delta G_{\text{solv}}$ (**10**) = –59.1 kcal/mol) is higher than that of the N<sub>1</sub>–CH<sub>3</sub> ligand ( $\Delta G_{\text{solv}}$ (**13**) = –56.0 kcal/mol). Thus, the additional energy penalty of **10** relative to **13**, due to solvation, must be compensated by additional interactions of **10** with the receptor. Thus, it seems reasonable to propose that the N<sub>1</sub>–H group of the benzimidazole ring acts as a hydrogen bond donor in the interaction with the receptor (see Molecular Model of the 5-HT<sub>4</sub>R–Ligand Interaction). Accordingly, the electrostatic map shows a blue (positive electron density enhances binding affinity) area at this position of the ring (see Figure 4a).

In regard to the basic amino moiety, the electrostatic map in Figure 4a shows a region in which positive charge enhances affinity (blue) near the nitrogen atom. The steric map illustrated in Figure 4b shows a large favorable (green) region of the terminus side chain into which the alkyl group of the (1-alkyl-4-piperidyl)-methylcarboxamides **5**, **6**, **8**–**19** or carboxylates **21**–**24** fits. The occupation of this area by a bulky group will have a positive effect on the biological affinity. Furthermore, the presence of at least one methylene unit between the acyl group and the piperidine ring is necessary for the binding at 5-HT<sub>4</sub> sites. Thus, analogues **1**–**4**, **7**, and **20** (no methylene unit) were either inactive or poorly active in 5-HT<sub>4</sub>R, and remarkably the alkyl group in these cases is not accommodated inside the green area. Also, analogues with a substituent at the nitrogen atom less voluminous than a butyl group are devoid of 5-HT<sub>4</sub>R affinity, except compound **7** ( $K_i$ (**7**)

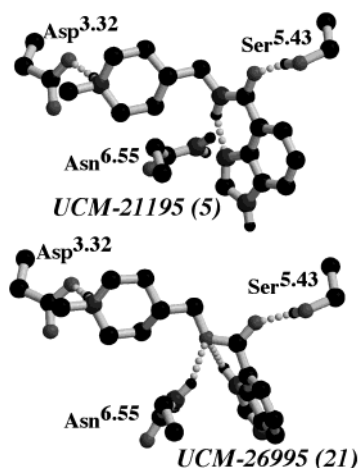


**Figure 5.** Ab initio geometry optimization of the antagonist binding site of the 5-HT<sub>4</sub>R composed of the side chains of Asp<sup>3.32</sup>, Ser<sup>5.43</sup>, and Asn<sup>6.55</sup> (nomenclature of Ballesteros and Weinstein<sup>27</sup>): (top) UCM-21195 (**5**); (bottom) UCM-26995 (**21**). Nonpolar hydrogens are not depicted to offer a better view of the recognition pocket. Figures were created using MolScript, version 2.1.1,<sup>59</sup> and Raster3D, version 2.5.<sup>60</sup>

= 54.0 nM) probably because of the presence of a chloro atom at the 6-position of the benzimidazole ring, since nonsubstituted analogue **1** shows a clear drop in binding affinity ( $K_i(\mathbf{1}) = 719$  nM). These results are in good agreement with our pharmacophore model for the 5-HT<sub>4</sub>R antagonist,<sup>22</sup> where both the presence of a voluminous substituent at the basic nitrogen of the amino moiety and the distance from this nitrogen to the aromatic ring are of great importance for high-affinity binding.

**Molecular Model of the 5-HT<sub>4</sub>R–Ligand Interaction.** The ligand binding site of the human 5-HT<sub>4</sub>R has structurally been explored by site-directed mutagenesis experiments.<sup>25</sup> This study has revealed that, among others, Ser<sup>5.43</sup>-Ala, Phe<sup>6.51</sup>-Ala, and Phe<sup>6.52</sup>-Val/Asn<sup>6.55</sup>-Leu mutants do not bind the GR113808 antagonist. Moreover, Asn<sup>6.55</sup>-Leu mutation reduces the affinity of GR113808 by a factor of 5.2. It has been suggested<sup>26</sup> from these results that GR113808 anchors the 5-HT<sub>4</sub>R mainly throughout the ionic interaction with Asp<sup>3.32</sup> and the hydrogen bond with Ser<sup>5.43</sup> and Asn<sup>6.55</sup>.

To identify the arrangement in space of the essential determinants for recognition of amide UCM-21195 (**5**) and ester UCM-26995 (**21**), we performed ab initio geometry optimization of the ligands inside the side chains of Asp<sup>3.32</sup>, Ser<sup>5.43</sup>, and Asn<sup>6.55</sup>. The positions of the C<sub>α</sub> atoms of the receptor side chains were kept fixed at the values obtained in the model of the transmembrane domain of the 5-HT<sub>4</sub>R (see Materials and Methods for computational details). Figure 5 depicts these energy-optimized structures. The antagonist–receptor complex is formed by (i) the ionic interaction between the NH group of the protonated piperidine and the O<sub>δ</sub> atom of Asp<sup>3.32</sup> at the optimized distance between heteroatoms of 2.55 Å (UCM-21195 (**5**)) or 2.50 Å (UCM-26995 (**21**)), (ii) the hydrogen bond between the carbonyl oxygen of the ligand and the hydroxyl group of Ser<sup>5.43</sup> (2.79 Å for UCM-21195 (**5**) and 3.06 Å for UCM-26995 (**21**)), (iii) the hydrogen bond between the hydrogens in the amide group of Asn<sup>6.55</sup> and the π electron clouds in the aromatic ring of the ligand at the optimized distance

between the heteroatom and the centroid of the ring of 3.69 Å (UCM-21195 (**5**)) or 4.10 Å (UCM-26995 (**21**)) (Figure 5). This hydrogen bond<sup>50</sup> is formed between the electron-rich π clouds of the aromatic ring of the ligand and the electron-poor hydrogens of Asn<sup>6.55</sup> in a manner similar to the proposed hydrogen bond between benzene and water<sup>51</sup> and benzene and ammonia.<sup>52</sup> Also, the electronic nature of the ether oxygen of UCM-26995 (**21**) facilitates, in contrast to the NH group of UCM-21195 (**5**), the hydrogen bond with both Asn<sup>6.55</sup> (3.25 Å) and the N<sub>3</sub>–H group of the benzimidazole ring (Figure 5). However, this additional hydrogen bond of UCM-26995 (**21**) with Asn<sup>6.55</sup> does not lead to a compound with higher affinity for the receptor ( $K_i(\mathbf{5}) = 13.7$  nM vs  $K_i(\mathbf{21}) = 24.6$  nM). This is attributed to the larger energy penalty of UCM-26995 (**21**) compared with that of UCM-21195 (**5**) ( $\Delta G_{\text{solv}}(\mathbf{21}) = -63.5$  kcal/mol vs  $\Delta G_{\text{solv}}(\mathbf{5}) = -58.7$  kcal/mol) to displace the ligand from the extracellular aqueous environment to the binding pocket of the receptor, and it is attributed to the energy required to change the conformation of UCM-26995 (**21**) from the **II**B conformation in free solution to the **II**A conformation in the bound state (see ref 32 and Materials and Methods).

These optimized reduced models of the ligand–receptor complex were used to position UCM-21195 (**5**) and UCM-26995 (**21**) inside the transmembrane domain of the 5-HT<sub>4</sub>R derived from the recently determined 3D structure of RHO<sup>44</sup> (see Materials and Methods for computational details). Figure 6 shows the antagonist binding pocket of the 5-HT<sub>4</sub>R for both ligands. The protonated piperidine of both ligands is located between Asp<sup>3.32</sup> and Phe<sup>6.51</sup> (Figure 6a shows these interactions for UCM-21195 (**5**)). The electron-rich clouds of the aromatic ring of Phe<sup>6.51</sup> interact with the electron-poor hydrogens of the carbon atoms adjacent to the protonated piperidine nitrogen of the ligand. This type of C–H⋯π interaction plays a significant role in stabilizing local 3D structures of proteins.<sup>53</sup> It has been shown that substitution of Phe<sup>6.51</sup> by Ala abolishes the binding of GR113808 to the 5-HT<sub>4</sub>R.<sup>25</sup> The importance of Phe<sup>6.51</sup> in the binding of the ligand is also reflected by the fact that substitution of Asp<sup>3.32</sup> by Asn does not decrease the affinity of piperidine-containing ligands such as GR113808.<sup>25</sup> The Asp<sup>3.32</sup>-Asn mutation decreases the binding to the NH moiety of the protonated piperidine, from an ion pair (Asp<sup>3.32</sup>) to a charged hydrogen bond (Asn), but increases the explicit charge in the hydrogens of the carbon atoms adjacent to the protonated piperidine nitrogen and accordingly the interaction with Phe<sup>6.51</sup>.<sup>26</sup> The absence of these hydrogen atoms in serotonin explains why the Asp<sup>3.32</sup>-Asn mutation has a significant effect in the binding of serotonin.<sup>25</sup> Moreover, the side chain of Asp<sup>3.32</sup> also forms a hydrogen bond with the neighboring side chain of Thr<sup>3.29</sup> (Figure 6a).

On the other hand, the benzimidazole ring of the UCM-21195 (**5**) and UCM-26995 (**21**) is located between Asn<sup>6.55</sup> and Tyr<sup>5.38</sup> (see parts b and c of Figure 6). The Tyr side chain is positioned in a face-to-edge orientation (T-shaped) to the benzimidazole ring. This type of π–σ aromatic–aromatic interaction has been described as a protein structure stabilization.<sup>54</sup> Moreover, the N<sub>1</sub>–H group of the benzimidazole ring of UCM-21195 (**5**) is pointing toward the O<sub>δ</sub> atom of Asn<sup>5.35</sup> (Figure 6b), and

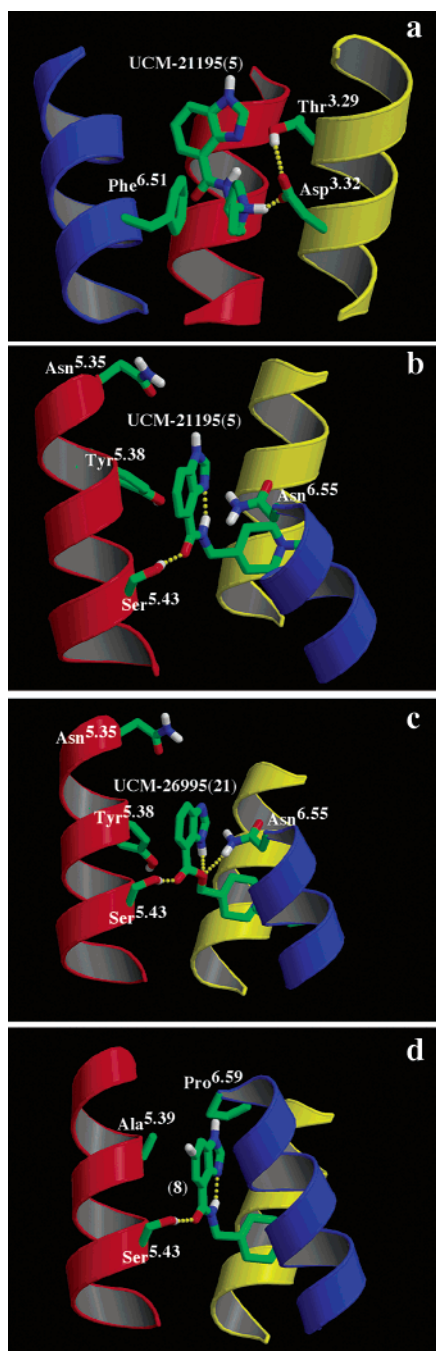


**Figure 6.** Molecular model of the transmembrane helix bundle of the 5-HT<sub>4</sub>R constructed from the 3D crystal structure of bovine rhodopsin.<sup>44</sup> The C<sub>α</sub> traces of the extracellular part (top) of TMHs 3 (yellow), 5 (red), and 6 (blue) are shown: (a, b) UCM-21195 (**5**); (c) UCM-26995 (**21**); (d) **8**. The 6-Cl substituted analogue of UCM-21195 is shown in the binding pocket in a detailed view of the ligand binding site. (a) The protonated piperidine of the ligand forms an ionic interaction with Asp<sup>3.32</sup> and a C–H···π hydrogen bond with Phe<sup>6.51</sup>. The side chain of Asp<sup>3.32</sup> also forms a hydrogen bond with the neighboring side chain of Thr<sup>3.29</sup>. (b, c) The carbonylic oxygen of the ligand forms a hydrogen bond with the hydroxyl group of Ser<sup>5.43</sup>, and the aromatic ring of the ligand forms a hydrogen bond with the NH group of Asn<sup>6.55</sup> and a π–σ stacking interaction with the benzene ring of Tyr<sup>5.38</sup>. The ether oxygen in the carboxylate UCM-26995 (**21**) forms a hydrogen bond with Asn<sup>6.55</sup>. (d) The 6-Cl atom (in white) is placed in a small cavity between Ala<sup>5.39</sup> and Pro<sup>6.59</sup>. Nonpolar hydrogens are not depicted to offer a better view of the recognition pocket. Figures were created using MolScript, version 2.1.1,<sup>59</sup> and Raster3D, version 2.5.<sup>60</sup>

the N<sub>1</sub> atom of UCM-26995 (**21**) is pointing toward the N<sub>δ</sub> atom Asn<sup>5.35</sup> (Figure 6c). It is important to note that the position of this residue in the molecular model of the 5-HT<sub>4</sub>R is very arbitrary. We have made the assumption that TMH 5 extends to position 5.35. This is based on the observation that TMH 5 prolongs to this residue in the 3D structure of RHO. However, 5-HT<sub>4</sub>R possesses a Pro residue at position 5.37, absent in the RHO structure. Pro is mostly located in loop regions in both soluble<sup>55</sup> and membrane proteins,<sup>56</sup> acting as helix breaker that might induce the Asn<sup>5.35</sup> backbone to adopt a conformation different from helical. This might locate the Asn<sup>5.35</sup> side chain closer to the ligand binding site than in the present model or totally away. However, the fact that methylation of the N<sub>1</sub>–H moiety of compound **10** results in a reduction of binding affinity suggests a direct hydrogen bond interaction with the receptor (see 3D-QSAR/CoMFA Model).

The superimposition of the CoMFA electrostatic and steric plots (see Figure 4) in the modeled 5-HT<sub>4</sub>R binding site shows that the green and red areas at the 6-position of the benzimidazole ring, where the Cl/Br atom are present, are located between TMHs 5 and 6. Thus, the hydrogen bond of the carbonyl group to Ser<sup>5.43</sup> positions the halogen atom between Ala<sup>5.39</sup>, located four residues apart from Ser<sup>5.43</sup> and thus in the same face of the helix, and Pro<sup>6.59</sup> (see Figure 6d). Analysis of the conservation pattern at the 5.39 position of all GPCR sequences denoted as serotonin (88 entries) in GPCRDB,<sup>57</sup> as of November 2001, shows that Ala is only present in the 5-HT<sub>4</sub>R, with the exception of the 5-HT<sub>5</sub>R. The other serotonin subtypes possess bulkier residues at this position: 5-HT<sub>1</sub> (Thr), 5-HT<sub>2</sub> (Val, Met), 5-HT<sub>5</sub> (Ala, Thr), 5-HT<sub>6</sub> (Val), and 5-HT<sub>7</sub> (Thr). Thus, this small cavity between TMHs 5 and 6 (see Figure 6d) is only present in the 5-HT<sub>4</sub>R and in some species of the 5-HT<sub>5</sub>R. Thus, the higher stabilization in the receptor binding site of the 6-halogen substituted ligands can be attributed to the additional electrostatic and van der Waals interaction of the halogen atom in this pocket located in transmembrane domains 5 and 6. Surprisingly, the effect of the chloro atom in the binding affinity is larger for carboxamides than for carboxylates (see 3D-QSAR/CoMFA Model). The hydrogen bond between the π electron clouds of the benzimidazole ring of the carboxamide UCM-21195 (**5**) and Asn<sup>6.55</sup> (see Figure 6b) optimally places the chloro atom inside the small cavity between TMHs 5 and 6 (see Figure 6d), whereas the hydrogen bond between the ether oxygen of the carboxylate UCM-26995 (**21**) and Asn<sup>6.55</sup> (see Figure 6c) places the chloro atom slightly toward TMH 5 (results not shown). This small change in the orientation of the chloro atom explains the different effect of 6-halogen substitution in carboxamides and carboxylates.

## Conclusions

3D-QSAR/CoMFA methodology and computational simulation of ligand recognition have been successfully applied to explain the 5HT<sub>4</sub>R binding affinities of a series of benzimidazole-4-carboxylic acid derivatives of piperidine **1–24**, which represent a class of 5-HT<sub>4</sub>R antagonists. Both derived computational models have facilitated the identification of the structural elements of the ligands that are key to high 5-HT<sub>4</sub>R affinity. The

most salient features of the electrostatic and steric maps obtained with the 3D-QSAR/CoMFA methodology are (i) a region near the protonated nitrogen of the piperidine ring in which positive charge density enhances binding affinity, (ii) a large favorable region near the piperidine ring into which voluminous substituents can be accommodated, (iii) a small favorable area at the 6-position of the benzimidazole ring into which high electron density substituents such as chloro and bromo enhance binding affinity, and (iv) unfavorable areas at the 7- and 1-N positions of the benzimidazole ring. On the other hand, the computational complexes between these ligands and the 5-HT<sub>4</sub>R show the following interactions: (i) the ionic interaction between the NH group of the protonated piperidine of the ligand and the carboxylate group of Asp<sup>3,32</sup>, (ii) the hydrogen bond between the carbonyl oxygen of the ligand and the hydroxyl group of Ser<sup>5,43</sup>, (iii) the hydrogen bond between the NH group of Asn<sup>6,55</sup> and the aromatic ring of carboxamides or the ether oxygen of carboxylates, (iv) the interaction of the electron-rich clouds of the aromatic ring of Phe<sup>6,51</sup> and the electron-poor hydrogens of the carbon atoms adjacent to the protonated piperidine nitrogen of the ligand, and finally (v) the  $\pi$ - $\sigma$  stacking interaction between the benzimidazole system of the ligand and the benzene ring of Tyr<sup>5,38</sup>. These results provide the tools for predicting the affinity of related compounds and for guiding the design and synthesis of new ligands with predetermined affinities and selectivity. These studies are now in progress, and the results will be reported in due course.

## Experimental Section

**Chemistry.** Melting points (uncorrected) were determined on a Gallenkamp electrothermal apparatus. <sup>1</sup>H and <sup>13</sup>C NMR spectra were recorded on a Varian VXR-300S or Bruker 300-AM instrument at 300 and 75 MHz, respectively, on a Bruker 250-AM spectrometer at 250 and 62.5 MHz, respectively, or on a Bruker 200-AC at 200 and 50 MHz, respectively. Chemical shifts ( $\delta$ ) are expressed in parts per million relative to internal tetramethylsilane. Coupling constants ( $J$ ) are in hertz (Hz). The following abbreviations are used to describe peak patterns when appropriate: s (singlet), d (doublet), t (triplet), m (multiplet), br (broad), ap (apparent). Elemental analyses (C, H, N) were determined at the UCM's analysis services, and the results were within  $\pm 0.4\%$  of the theoretical values. Analytical thin-layer chromatography (TLC) was run on Merck silica gel plates (Kieselgel 60 F-254) with detection by UV light, iodine, acidic vanillin solution, or 10% phosphomolybdic acid solution in ethanol. For flash chromatography, Merck silica gel type 60 (size 230–400 mesh) was used. Unless stated otherwise, all starting materials and reagents were high-grade commercial products purchased from Aldrich, Fluka, or Merck. All solvents were distilled prior to use. Dry DMF was obtained by stirring with CaH<sub>2</sub> followed by distillation under argon.

The benzimidazole-4-carboxylic acids **25–27**<sup>33</sup> and (1-butyl-4-piperidyl)methylamine (**28**)<sup>24</sup> were synthesized according to the literature.

**General Procedure for the Synthesis of Benzimidazole-4-carboxamides (14–16).** To a solution of acids **25–27** (5 mmol) in dry DMF (5 mL) under an argon atmosphere was added 1,1'-carbonyldiimidazole (CDI, 811 mg, 5 mmol). The mixture was stirred at 40 °C for 1 h, and then a solution of 1.02 g (6 mmol) of (1-butyl-4-piperidyl)methylamine (**28**) and 1,8-diazabicyclo[5.4.0]undec-7-ene (DBU, 761 mg, 5 mmol) in DMF (10 mL) was added dropwise, and the reaction mixture was stirred at 50 °C for 20–24 h. The solvent was removed under reduced pressure, and the crude was taken up in CHCl<sub>3</sub> (50 mL) and washed with water (20 mL) and 20% aqueous

K<sub>2</sub>CO<sub>3</sub> (20 mL). The organic layer was dried over Na<sub>2</sub>SO<sub>4</sub> or MgSO<sub>4</sub> and was evaporated to afford the crude product, which was purified by column chromatography and recrystallization from the appropriate solvents.

**N-[(1-Butyl-4-piperidyl)methyl]-6-bromobenzimidazole-4-carboxamide (14):** yield 35%; chromatography from AcOEt to AcOEt/EtOH, 4:1; mp 182–184 °C (d) (toluene); <sup>1</sup>H NMR (DMSO-*d*<sub>6</sub>)  $\delta$  0.89 (t,  $J$  = 7.5, 3H), 1.20–1.44 (m, 6H), 1.58 (m, 1H), 1.72 (d,  $J$  = 12.3, 2H), 1.87 (t,  $J$  = 10.2, 2H), 2.27 (ap t,  $J$  = 6.6, 2H), 2.89 (d,  $J$  = 11.1, 2H), 3.35 (br t,  $J$  = 6.3, 2H), 7.97 (s, 1H), 8.00 (d,  $J$  = 1.2, 1H), 8.50 (s, 1H), 9.66 (br s, 1H); <sup>13</sup>C NMR (DMSO-*d*<sub>6</sub>)  $\delta$  14.0, 20.2, 28.6, 29.7, 36.0, 44.6, 53.1, 57.9, 114.3, 119.1, 123.0, 124.6, 137.0, 137.9, 144.3, 163.6. Anal. (C<sub>18</sub>H<sub>25</sub>BrN<sub>4</sub>O) C, H, N.

**N-[(1-Butyl-4-piperidyl)methyl]-6-chloro-7-nitrobenzimidazole-4-carboxamide (15):** yield 84%; chromatography from CHCl<sub>3</sub> to CHCl<sub>3</sub>/MeOH, 9:1; mp 188–190 °C (d) (AcOEt); <sup>1</sup>H NMR (DMSO-*d*<sub>6</sub>)  $\delta$  0.88 (t,  $J$  = 7.1, 3H), 1.18–1.55 (m, 6H), 1.60–1.81 (m, 3H), 2.31 (br t,  $J$  = 12.2, 2H), 2.57 (ap t,  $J$  = 7.1, 2H), 3.13 (br d,  $J$  = 12.4, 2H), 3.35 (br t,  $J$  = 5.9, 2H), 7.82 (s, 1H), 8.31 (s, 1H), 9.93 (br s, 1H); <sup>13</sup>C NMR (DMSO-*d*<sub>6</sub>)  $\delta$  13.8, 19.9, 27.2, 28.4, 35.0, 44.1, 52.3, 56.8, 115.0, 120.4, 122.9, 136.4, 137.9, 141.1, 151.3, 163.4. Anal. (C<sub>18</sub>H<sub>24</sub>ClN<sub>5</sub>O<sub>3</sub>) C, H, N.

**N-[(1-Butyl-4-piperidyl)methyl]-6-bromo-7-nitrobenzimidazole-4-carboxamide (16):** yield 95%; chromatography from CHCl<sub>3</sub> to CHCl<sub>3</sub>/MeOH, 4:1; mp 189–190 °C (d) (AcOEt); <sup>1</sup>H NMR (DMSO-*d*<sub>6</sub>)  $\delta$  0.88 (t,  $J$  = 7.1, 3H), 1.18–1.55 (m, 6H), 1.60–1.81 (m, 3H), 2.30 (br t,  $J$  = 11.7, 2H), 2.56 (ap t,  $J$  = 7.6, 2H), 3.12 (br d,  $J$  = 11.7, 2H), 3.34 (br t,  $J$  = 5.9, 2H), 7.96 (s, 1H), 8.28 (s, 1H), 9.86 (br s, 1H); <sup>13</sup>C NMR (DMSO-*d*<sub>6</sub>)  $\delta$  13.7, 19.8, 27.2, 28.4, 35.0, 44.0, 52.3, 56.8, 102.3, 122.9, 123.1, 136.8, 140.1, 141.0, 150.9, 163.4. Anal. (C<sub>18</sub>H<sub>24</sub>BrN<sub>5</sub>O<sub>3</sub>) C, H, N.

**General Procedure for the Synthesis of 7-Amino-6-halobenzimidazole-4-carboxamides (17, 18).** To a solution of **15** or **16** (0.75 mmol) in ethanol (15 mL), Raney nickel and 80% hydrazine hydrate (0.1 mL, 0.002 mmol) were added dropwise. The reaction mixture was stirred for 15 min and filtered through Celite. The solvent was removed under reduced pressure, and the residue was purified by column chromatography.

**N-[(1-Butyl-4-piperidyl)methyl]-7-amino-6-chlorobenzimidazole-4-carboxamide (17):** yield 39%; chromatography CHCl<sub>3</sub>/MeOH/NH<sub>3</sub>, from 9.5:0.5:0.1 to 9:1:0.1; mp 232–234 °C (d) (CHCl<sub>3</sub>); <sup>1</sup>H NMR (DMSO-*d*<sub>6</sub>)  $\delta$  0.89 (t,  $J$  = 7.2, 3H), 1.19–1.46 (m, 6H), 1.55 (m, 1H), 1.70 (br d,  $J$  = 12.3, 2H), 1.89 (br t,  $J$  = 11.4, 2H), 2.28 (ap t,  $J$  = 7.6, 2H), 2.89 (br d,  $J$  = 10.5, 2H), 3.27 (m, 2H), 6.08 (s, 2H), 7.79 (s, 1H), 8.39 (br s, 1H), 9.57 (br s, 1H), 12.41 (br s, 1H); <sup>13</sup>C NMR (DMSO-*d*<sub>6</sub>)  $\delta$  13.9, 20.1, 28.5, 29.7, 36.4, 44.3, 53.1, 57.8, 109.2, 111.8, 124.5, 131.8, 134.3, 139.9, 141.7, 164.4. Anal. (C<sub>18</sub>H<sub>26</sub>ClN<sub>5</sub>O) C, H, N.

**N-[(1-Butyl-4-piperidyl)methyl]-7-amino-6-bromobenzimidazole-4-carboxamide (18):** yield 51%; chromatography CHCl<sub>3</sub>/MeOH/NH<sub>3</sub>, from 9.5:0.5:0.1 to 8:2:0.1; mp 228–230 °C (d) (CHCl<sub>3</sub>); <sup>1</sup>H NMR (DMSO-*d*<sub>6</sub>)  $\delta$  0.89 (t,  $J$  = 8.1, 3H), 1.18–1.47 (m, 6H), 1.55 (m, 1H), 1.70 (br d,  $J$  = 12.3, 2H), 1.88 (br t,  $J$  = 11.1, 2H), 2.28 (ap t,  $J$  = 7.2, 2H), 2.89 (br d,  $J$  = 11.4, 2H), 3.27 (m, 2H), 6.10 (s, 2H), 7.89 (s, 1H), 8.36 (br s, 1H), 9.54 (br s, 1H), 12.38 (br s, 1H); <sup>13</sup>C NMR (DMSO-*d*<sub>6</sub>)  $\delta$  13.9, 20.2, 28.5, 29.7, 36.1, 44.3, 53.1, 57.8, 98.0, 111.9, 121.4, 127.1, 131.8, 135.2, 141.4, 164.5. Anal. (C<sub>18</sub>H<sub>26</sub>BrN<sub>5</sub>O) C, H, N.

**N-[(1-Butyl-4-piperidyl)methyl]-7-aminobenzimidazole-4-carboxamide (19).** A solution of **16** (260 mg, 0.59 mmol) in ethanol (12 mL) was warmed to 60 °C. Then 10% Pd(C) (72 mg, 0.07 mmol) and 80% hydrazine hydrate (1.65 mL, 0.03 mmol) were added dropwise, and the mixture was refluxed for 30 min. The solvent was removed under reduced pressure, and the residue was purified by column chromatography (CHCl<sub>3</sub>/MeOH/NH<sub>3</sub>, from 9.5:0.5:0.1 to 8:2:0.1) to yield 175 mg (90%) of **19**: mp 162–164 °C (d); <sup>1</sup>H NMR (DMSO-*d*<sub>6</sub>)  $\delta$  0.90 (t,  $J$  = 7.5, 3H), 1.18–1.50 (m, 6H), 1.57 (m, 1H), 1.73 (br d,  $J$  = 12.3, 2H), 2.01 (br t,  $J$  = 11.4, 2H), 2.37 (ap t,  $J$  = 7.2, 2H), 2.97 (br

d,  $J = 11.7$ , 2H), 3.21 (m, 2H), 5.89 (s, 2H), 6.50 (d,  $J = 8.4$ , 1H), 7.65 (d,  $J = 8.1$ , 1H), 8.36 (s, 1H), 9.64 (br s, 1H), 12.19 (br s, 1H);  $^{13}\text{C}$  NMR (DMSO- $d_6$ )  $\delta$  13.9, 20.0, 27.9, 29.2, 35.8, 43.9, 52.7, 57.4, 104.5, 109.6, 121.7, 124.5, 135.2, 140.4, 165.9. Anal. ( $\text{C}_{18}\text{H}_{27}\text{N}_5\text{O}$ ) C, H, N.

**Radioligand Binding Assays at 5-HT<sub>4</sub>R.** Male Sprague–Dawley rats (*Rattus norvegicus albinus*), weighing 180–200 g, were killed by decapitation, and the brains were rapidly removed and dissected. Tissues were stored at  $-80^\circ\text{C}$  for subsequent use and homogenized on a Polytron PT-10 homogenizer. Membrane suspensions were centrifuged on a Beckman J2-HS instrument.

Binding assays were performed according to the procedure previously described by Grossman et al.<sup>34</sup> The striatum was homogenized in 15 volumes of ice-cold 50 mM HEPES buffer (pH 7.4 at  $4^\circ\text{C}$ ) and centrifuged at 48000g for 10 min. The pellet was resuspended in 4.5 mL of assay buffer (50 mM HEPES, pH 7.4 at  $4^\circ\text{C}$ ). Fractions of 100  $\mu\text{L}$  of the final membrane suspension were incubated at  $37^\circ\text{C}$  for 30 min with 0.1 nM [ $^3\text{H}$ ]GR113808 (85 Ci/mmol), in the presence or absence of six concentrations of the competing drug, in a final volume of 1 mL of assay buffer. Nonspecific binding was determined with 30  $\mu\text{M}$  5-HT and represented less than 40% of the total binding.

Competing drug, nonspecific, total, and radioligand bindings were defined in triplicate. Incubation was terminated by rapid vacuum filtration through Whatman GF/B filters presoaked in 0.05% poly(ethylenimine), using a Brandel cell harvester. The filters were then washed once with 4 mL of ice-cold 50 mM HEPES, pH 7.4, at  $4^\circ\text{C}$  and dried. The filters were placed in poly(ethylene) vials to which were added 4 mL of a scintillation cocktail (Aquasol), and the radioactivity bound to the filters was measured by liquid scintillation spectrometry. The data were analyzed by an iterative curve-fitting procedure (program Prism, Graph Pad), which provided  $\text{IC}_{50}$ ,  $K_i$ , and  $r^2$  values for test compounds,  $K_i$  values being calculated from the Cheng and Prusoff equation.<sup>35</sup> The protein concentrations of the rat cerebral cortex and the rat striatum were determined by the method of Lowry,<sup>58</sup> using bovine serum albumin as the standard.

**Acknowledgment.** This work was supported by the Ministerio de Ciencia y Tecnología (Grant BQU2001-1459), the CICYT (Grant SAF99-073), the DGEIC (Grant PB97-0282), the Universidad Complutense (Grant PR486/97-7483), and Fundació La Marató TV (Grant 0014/97). Some of the simulations were run at the Centre de Computació i Comunicacions de Catalunya. The authors are grateful to Universidad Complutense for a predoctoral grant to M. Murcia.

## References

- Bockaert, J.; Fagni, L.; Dumuis, A. 5-HT<sub>4</sub> receptors: an update. In *Serotonergic Neurons and 5-HT Receptors in the CNS*; Baumgarten, H. G., Göthert, M., Eds.; Springer-Verlag: Berlin, 1997; pp 439–474.
- Hoyer, D.; Martin, G. 5-HT receptor classification and nomenclature: towards a harmonization with the human genome. *Neuropharmacology* **1997**, *36*, 419–428.
- Uphouse, L. Multiple serotonin receptors: too many, not enough, or just the right number? *Neurosci. Biobehav. Rev.* **1997**, *21*, 679–698.
- Murphy, D. L.; Andrews, A. M.; Wichems, C. H.; Li, Q.; Tohda, M.; Greenberg, B. Brain serotonin neurotransmission: an overview and update with an emphasis on serotonin subsystem heterogeneity, multiple receptors, interactions with other neurotransmitter systems, and consequent implications for understanding the actions of serotonergic drugs. *J. Clin. Psychiatry* **1988**, *59* (Suppl. 15), 4–12.
- Saxena, P. R.; De Vries, P.; Villalon, C. M. 5-HT<sub>1</sub>-like receptors: a time to bid goodbye. *Trends Pharmacol. Sci.* **1998**, *19*, 311–316.
- Fagni, L.; Dumuis, A.; Sebben, M.; Bockaert, J. The 5-HT<sub>4</sub> receptor subtype inhibits K<sup>+</sup> current in colliculi neurones via activation of a cyclic AMP-dependent protein kinase. *Br. J. Pharmacol.* **1992**, *105*, 973–979.
- Eglen, R. M.; Swank, S. R.; Walsh, L. K.; Whiting, R. L. Characterization of 5-HT<sub>3</sub> and "atypical" 5-HT receptors mediating guinea-pig ileal contractions in vitro. *Br. J. Pharmacol.* **1990**, *101*, 513–520.
- McLean, P. G.; Coupar, I. M.; Molenaar, P. A comparative study of functional 5-HT<sub>4</sub> receptors in human colon, rat oesophagus and rat ileum. *Br. J. Pharmacol.* **1995**, *115*, 47–56.
- Matsuyama, S.; Sakiyama, H.; Nei, K.; Tanaka, C. Identification of putative 5-hydroxytryptamine<sub>4</sub> (5-HT<sub>4</sub>) receptors in guinea pig stomach: The effect of TKS159, a novel agonist, on gastric motility and acetylcholine release. *J. Pharmacol. Exp. Ther.* **1996**, *276*, 989–995.
- Villalon, C. M.; den Boer, M. O.; Heiligers, J. P.; Saxena, P. R. Mediation of 5-hydroxytryptamine-induced tachycardia in the pig by the putative 5-HT<sub>4</sub> receptor. *Br. J. Pharmacol.* **1990**, *100*, 665–667.
- Candura, S. M.; Messori, E.; Franceschetti, G. P.; D'Agostino, G.; Vicini, D.; Tagliani, M.; Tonini, M. Neural 5-HT<sub>4</sub> receptors in the human isolated detrusor muscle: effects of indole, benzimidazolone and substituted benzamide agonists and antagonists. *Br. J. Pharmacol.* **1996**, *118*, 1965–1970.
- Briejer, M. R.; Akkermans, L. M.; Schuurkes, J. A. Gastrointestinal prokinetic benzamides: the pharmacology underlying stimulation of motility. *Pharmacol. Rev.* **1995**, *47*, 631–651.
- Samrna, S. K.; Briejer, M. R.; Schuurkes, J. A. J. 5-HT<sub>3</sub>/5-HT<sub>4</sub> receptors in motility disorders: New therapeutic agents. In *Drug development: molecular targets for GI diseases*; Gagliella, T. S., Guglietta, A., Eds.; Humana Press Inc.: Totowa, NJ, 2000; pp 177–202.
- Hedge, S. S.; Moy, T. M.; Perry, M. R.; Loeb, M.; Eglen, R. M. Evidence for the involvement of 5-hydroxytryptamine<sub>4</sub> receptors in 5-hydroxytryptophan-induced diarrhea in mice. *J. Pharmacol. Exp. Ther.* **1994**, *271*, 741–747.
- Farthing, M. J. G. New drugs in the management of the irritable bowel syndrome. *Drugs* **1998**, *56*, 11–21.
- Farthing, M. J. G. Irritable bowel syndrome: new pharmaceutical approaches to treatment. *Best Pract. Res. Clin. Gastroenterol.* **1999**, *13*, 461–471.
- Kaumann, A. J. Do human atrial 5-HT<sub>4</sub> receptors mediate arrhythmias? *Trends Pharmacol. Sci.* **1994**, *S15*, 451–455.
- Tonini, M.; Candura, S. M. 5-HT<sub>4</sub> receptor agonists and bladder disorders. *Trends Pharmacol. Sci.* **1996**, *17*, 314–316.
- Ferguson, D.; Christopher, N. Urinary bladder function and drug development. *Trends Pharmacol. Sci.* **1996**, *17*, 161–165.
- Eglen, R. M.; Wong, E. H.; Dumuis, A.; Bockaert, J. Central 5-HT<sub>4</sub> receptors. *Trends Pharmacol. Sci.* **1995**, *16*, 391–398.
- Gaster, L. M.; King, F. D. Serotonin 5-HT<sub>3</sub> and 5-HT<sub>4</sub> receptor antagonists. *Med. Res. Rev.* **1997**, *17*, 163–214.
- López-Rodríguez, M. L.; Morcillo, M. J.; Benhamú, B.; Rosado, M. L. Comparative receptor mapping of serotonergic 5-HT<sub>3</sub> and 5-HT<sub>4</sub> binding sites. *J. Comput.-Aided Mol. Des.* **1997**, *11*, 589–599.
- López-Rodríguez, M. L.; Morcillo, M. J.; Benhamú, B. Nuevos derivados de benzimidazol con afinidad por los receptores serotonérgicos 5-HT<sub>3</sub>/5-HT<sub>4</sub>. Patent PCT/ES97/00068, WO 97/35860, 1997; *Chem. Abstr.* **1997**, *127* (4), 331485n.
- López-Rodríguez, M. L.; Benhamú, B.; Viso, A.; Morcillo, M. J.; Murcia, M.; Orensanz, L.; Alfaro, M. J.; Martín, M. I. Benzimidazole derivatives. Part I: Synthesis and structure–activity relationships of new benzimidazole-4-carboxamides and carboxylates as potent and selective 5-HT<sub>4</sub> receptor antagonists. *Bioorg. Med. Chem.* **1999**, *7*, 2271–2281.
- Mialet, J.; Dahmoune, Y.; Lezoualc'h, F.; Berque-Bestel, I.; Eftekhari, P.; Hoebeke, J.; Sicsic, S.; Langlois, M.; Fischmeister, R. Exploration of the ligand binding site of the human 5-HT<sub>4</sub> receptor by site-directed mutagenesis and molecular modeling. *Br. J. Pharmacol.* **2000**, *130*, 527–538.
- López-Rodríguez, M. L.; Murcia, M.; Benhamú, B.; Olivella, M.; Campillo, M.; Pardo, L. Computational model of the complex between GR113808 and the 5-HT<sub>4</sub> receptor guided by site-directed mutagenesis and the crystal structure of rhodopsin. *J. Comput.-Aided Mol. Des.* **2001**, *15*, 1025–1033.
- Ballesteros, J. A.; Weinstein, H. Integrated methods for the construction of three-dimensional models and computational probing of structure–function relations in G protein-coupled receptors. *Methods Neurosci.* **1995**, *25*, 366–428.
- López-Rodríguez, M. L.; Murcia, M.; Benhamú, B.; Viso, A.; Campillo, M.; Pardo, L. 3-D-QSAR/CoMFA and recognition models of benzimidazole derivatives at the 5-HT<sub>4</sub> receptor. *Bioorg. Med. Chem. Lett.* **2001**, *11*, 2807–2811.
- Green, S. M.; Marshall, G. R. 3D-QSAR: a current perspective. *Trends Pharmacol. Sci.* **1995**, *16*, 285–291.
- Cramer, R. D.; Patterson, D. E.; Bunce, J. D. Comparative molecular field analysis (CoMFA). 1. Effect of shape on binding of steroids to carrier proteins. *J. Am. Chem. Soc.* **1988**, *110*, 5959–5967.

- (31) Clark, M.; Cramer, R. D. I.; Jones, D. M.; Patterson, D. E.; Simeroth, P. E. Comparative molecular field analysis (CoMFA). 2. Toward its use with 3D-structural databases. *Tetrahedron Comput. Methodol.* **1990**, *3*, 47–59.
- (32) López-Rodríguez, M. L.; Benhamú, B.; Viso, A.; Murcia, M.; Pardo, L. Study of the bioactive conformation of novel 5-HT<sub>4</sub> receptor ligands: influence of an intramolecular hydrogen bond. *Tetrahedron* **2001**, *57*, 6745–6749.
- (33) López-Rodríguez, M. L.; Benhamú, B.; Morcillo, M. J.; Tejada, I. D.; Orensanz, L.; Alfaro, M. J.; Martín, M. I. Benzimidazole derivatives. 2. Synthesis and structure–activity relationships of new azabicyclic benzimidazole-4-carboxylic acid derivatives with affinity for serotonergic 5-HT<sub>3</sub> receptors. *J. Med. Chem.* **1999**, *42*, 5020–5028.
- (34) Grossman, C. J.; Kilpatrick, G. J.; Bunce, K. T. Development of a radioligand binding assay for 5-HT<sub>4</sub> receptors in guinea-pig and rat brain. *Br. J. Pharmacol.* **1993**, *109*, 618–624.
- (35) Cheng, Y.; Prusoff, W. H. Relationship between the inhibition constant (*K*) and the concentration of inhibitor which causes 50 per cent inhibition (*IC*<sub>50</sub>) of an enzymatic reaction. *Biochem. Pharmacol.* **1973**, *22*, 3099–3108.
- (36) Singh, U. C.; Kollman, P. A. An approach to computing electrostatic charges for molecules. *J. Comput. Chem.* **1984**, *5*, 129–145.
- (37) Cornell, W. D.; Cieplak, P.; Bayly, C.; Gould, I. R.; Merz, K. M.; Ferguson, D. M.; Spellmeyer, D. C.; Fox, T.; Caldwell, J. W.; Kollman, P. A. A second generation force field for the simulation of proteins, nucleic acids, and organic molecules. *J. Am. Chem. Soc.* **1995**, *117*, 5179–5197.
- (38) Dunn, W. J.; Wold, S.; Edlund, U.; Hellberg, S.; Gasteiger, J. Multivariate structure–activity relationships between data from a battery of biological tests and an ensemble of structure descriptors: the PLS method. *Quant. Struct.–Act. Relat.* **1984**, *3*, 131–137.
- (39) Wold, S.; Ruhe, A.; Wold, H.; Dunn, W. J. I. The covariance problem in linear regression. The partial least squares (PLS) approach to generalized inverses. *SIAM J. Sci. Stat. Comput.* **1984**, *5*, 735–743.
- (40) Cramer, R. D.; Bunce, J. D.; Patterson, D. E. Crossvalidation, bootstrapping and partial least squares compared with multiple regression in conventional QSAR studies. *Quant. Struct.–Act. Relat.* **1988**, *7*, 18–25.
- (41) Wold, S.; Albano, C.; Dunn, W. J. I.; Edlund, U.; Esbensen, W.; Geladi, P.; Hellberg, S.; Johansson, E.; Lindberg, W.; Sjöström, M. Multivariate data analysis in chemistry. In *Chemometrics: mathematics and statistics in chemistry*; Kowwalsky, B. R., Ed.; Reidel: Dordrecht, The Netherlands, 1984; pp 17–95.
- (42) SYBYL, version 6.6: Tripos Inc., 1699 South Hanley Road, St. Louis, MO 63144.
- (43) Frisch, M. J.; Trucks, G. W.; Schlegel, H. B.; Scuseria, G. E.; Robb, M. A.; Cheeseman, J. R.; Zakrzewski, V. G.; Montgomery, J. A., Jr.; Stratmann, R. E.; Burant, J. C.; Dapprich, S.; Millam, J. M.; Daniels, A. D.; Kudin, K. N.; Strain, M. C.; Farkas, O.; Tomasi, J.; Barone, V.; Cossi, M.; Cammi, R.; Mennucci, B.; Pomelli, C.; Adamo, C.; Clifford, S.; Ochterski, J.; Petersson, G. A.; Ayala, P. Y.; Cui, Q.; Morokuma, K.; Malick, D. K.; Rabuck, A. D.; Raghavachari, K.; Foresman, J. B.; Cioslowski, J.; Ortiz, J. V.; Stefanov, B. B.; Liu, G.; Liashenko, A.; Piskorz, P.; Komaromi, I.; Gomperts, R.; Martin, R. L.; Fox, D. J.; Keith, T.; Al-Laham, M. A.; Peng, C. Y.; Nanayakkara, A.; Gonzalez, C.; Challacombe, M.; Gill, P. M. W.; Johnson, B. G.; Chen, W.; Wong, M. W.; Andres, J. L.; Head-Gordon, M.; Replogle, E. S.; Pople, J. A. *Gaussian 98*; Gaussian, Inc.: Pittsburgh, PA, 1998.
- (44) Palczewski, K.; Kumasaka, T.; Hori, T.; Behnke, C. A.; Motoshima, H.; Fox, B. A.; Le Trong, I.; Teller, D. C.; Okada, T.; Stenkamp, R. E.; Yamamoto, M.; Miyano, M. Crystal structure of rhodopsin: A G protein-coupled receptor. *Science* **2000**, *289*, 739–745.
- (45) Dunbrack, R. L.; Cohen, F. E. Bayesian statistical analysis of protein side-chain rotamer preferences. *Protein Sci.* **1997**, *6*, 1661–1681.
- (46) Ballesteros, J. A.; Deupi, X.; Olivella, M.; Haaksma, E. E.; Pardo, L. Serine and threonine residues bend  $\alpha$ -helices in the  $\chi_1 = g^-$  conformation. *Biophys. J.* **2000**, *79*, 2754–2760.
- (47) López-Rodríguez, M. L.; Vicente, B.; Deupi, X.; Barrondo, S.; Olivella, M.; Morcillo, M. J.; Benhamú, B.; Ballesteros, J. A.; Sallés, J.; Pardo, L. Design, synthesis and pharmacological evaluation of 5-hydroxytryptamine<sub>1A</sub> receptor ligands to explore the three-dimensional structure of the receptor. *Mol. Pharmacol.* **2002**, *62*, 15–21.
- (48) Case, D. A.; Pearlman, D. A.; Caldwell, J. W.; Cheatham, T. E.; Ross, W. S.; Simmerling, T. A.; Darden, T. A.; Merz, K. M.; Stanton, R. V.; Cheng, A. L.; Vicent, J. J.; Crowley, M.; Ferguson, D. M.; Radmer, R. J.; Seibel, G. L.; Singh, U. C.; Weiner, P. K.; Kollman, P. A. *AMBER 5*; University of California, San Francisco, 1997.
- (49) Cieplak, P.; Cornell, W. D.; Bayly, C.; Kollman, P. A. Application of the multimolecule and multiconformational RESP methodology to biopolymers: charge derivation for DNA, RNA, and proteins. *J. Comput. Chem.* **1995**, *16*, 1357–1377.
- (50) Levitt, M.; Perutz, M. F. Aromatic rings act as hydrogen bond acceptors. *J. Mol. Biol.* **1988**, *201*, 751–754.
- (51) Suzuki, S.; Green, P. G.; Bumgarner, R. E.; Dasgupta, S.; Goddard, W. A. I.; Blake, G. A. Benzene forms hydrogen bonds with water. *Science* **1992**, *257*, 942–945.
- (52) Rodham, D. A.; Suzuki, S.; Suenram, R. D.; Lovas, F. J.; Dasgupta, S.; Goddard, W. A. I.; Blake, G. A. Hydrogen bonding in the benzene–ammonia dimer. *Nature* **1993**, *362*, 735–737.
- (53) Steiner, T.; Koellner, G. Hydrogen bonds with  $\pi$ -acceptors in proteins: frequencies and role in stabilizing local 3D structures. *J. Mol. Biol.* **2001**, *305*, 535–557.
- (54) Burley, S. K.; Petsko, G. A. Aromatic–aromatic interaction: a mechanism of protein structure stabilization. *Science* **1985**, *229*, 23–28.
- (55) O’Neil, K. T.; DeGrado, W. F. A thermodynamic scale for the helix-forming tendencies of the commonly occurring amino acids. *Science* **1990**, *250*, 646–651.
- (56) Monne, M.; Hermansson, M.; von Heijne, G. A turn propensity scale for transmembrane helices. *J. Mol. Biol.* **1999**, *288*, 141–145.
- (57) Horn, F.; Weare, J.; Beukers, M. W.; Horsch, S.; Bairoch, A.; Chen, W.; Edvardsen, O.; Campagne, F.; Vriend, G. GPCRDB: an information system for G protein-coupled receptors. *Nucleic Acids Res.* **1998**, *26*, 275–279.
- (58) Lowry, O. H.; Rosebrough, N. J.; Farr, A. L.; Randall, R. J. Protein measurement with the folin phenol reagent. *J. Biol. Chem.* **1951**, *193*, 265–275.
- (59) Kraulis, P. J. MOLSCRIPT: a program to produce both detailed and schematic plots of protein structures. *J. Appl. Crystallogr.* **1991**, *24*, 945–950.
- (60) Merritt, E. A.; Bacon, D. J. Raster3D: photorealistic molecular graphics. *Methods Enzymol.* **1997**, *277*, 505–524.

JM020807X